

Successful Test of a Prototype Hadron Blind Detector

R.P. Pisani¹, T.K. Hemmick², H. Chung³, S.C. Johnson,
T. Piazza, T. Vongpaseuth

*Department of Physics, SUNY Stony Brook, Stony Brook New York 11974-3800,
USA*

M. Akopyan⁴

*Laboratory for Nuclear Science, Massachusetts Institute of Technology, Cambridge
Massachusetts*

We have constructed and tested a threshold Cherenkov detector inspired by the conceptual design of Giomataris and Charpak[1]. The basic design consists of a gas radiator followed by a photosensitive wire chamber using a solid CsI photocathode. The photon detector lies directly in the particle path and is required to have single photo-electron sensitivity and yet be insensitive to the passage of a charged particle. We have altered the design by adding a thin LiF window. This window allows one to separate the radiator and avalanche volumes, giving greater flexibility in the gas choices. Our detector was operated with C_2F_6 as the radiator gas at lengths of 120, 80, and 40 cm. The avalanche gas was 95% He + 5% CH_4 . At 95% electron efficiency, the pion efficiency was 1/333, 1/150, and 1/100 for each of the lengths listed above.

1 Introduction

As high energy and nuclear physics experiments evolve toward the detection of higher particle densities, the need for particle species selection directly in hardware becomes increasingly acute. A Cherenkov detector operated in threshold mode is the textbook example of a species dependent detector. However,

¹ Present Address: Department of Physics, Brookhaven National Lab

² Corresponding Author

³ Present Address: Department of Physics, Smith College

⁴ on leave from Institute for Nuclear Research, Moscow, Russia.

Cherenkov detectors are difficult to implement in a compact layered or hermetic detector due to the need for focusing optics (which often create dead detector space), long radiator lengths, and thickness (in radiation lengths) of the photo-sensitive layer.

During the past several years solid CsI photocathode wire chamber techniques have shown increasing promise[2–6]. Rings have been successfully observed in mirror focusing[7] and proximity focusing[8–10] configurations. Additionally, the initially disparate reports on quantum efficiency (QE)[11–13] have somewhat converged[9,14–16] as photocathode production techniques[2,17,18] and QE measurement standards have been improved[19].

An especially interesting configuration of a CsI photocathode Cherenkov detector was suggested by Giomataris and Charpak in 1991[1]. A sketch of this design is shown in the top panel of Figure 1. Charged particles pass through the radiator gas. Cherenkov photons created by particles above threshold ($v > c/n$) pass through the anode mesh and are intercepted by the cathode. Photo-electrons created at the cathode avalanche toward the anode in a Parallel-Plate Avalanche Counter (PPAC) gap. This “windowless” configuration maximizes the photo-electron yield since the low wavelength cutoff is set by the transmission properties of the gas, not by a window. When run in threshold mode, the detector can be set to be sensitive to electrons and insensitive to pions and higher mass particles and has thus been dubbed a Hadron Blind Detector or HBD.

The requirements on the HBD radiator gas are severe. The gas must simultaneously provide a high index of refraction, excellent transparency, good avalanche characteristics, and chemical compatibility with the photocathode. An experiment using pure CF_4 as the operating gas met with only limited success. CF_4 gas does provide a high index of refraction ($n=1.000620$) and excellent transparency (down to 120 nm). If the avalanche gas should crack, however, the fragments can often be highly electronegative. It is presently suspected that the relatively small electron signal found in this configuration is the result of absorption of photo-electrons prior to avalanche, frequently and effectively eliminating the signal. Additionally, there could be detrimental chemical interactions between the CsI layer and free F^- ions created during avalanche[14], making CF_4 a less than optimal avalanche gas choice.

We have altered the HBD design to include a very thin LiF window to separate the radiator from the avalanche gas (as shown in the bottom panel of Figure 1). At 0.5 mm thickness, the window accounts for very little material ($.5\text{mm}/X_o=0.3\%$)⁵ and thereby does not violate the requirement that the detector be low

⁵ Here X_o is the radiation length of the material and is defined as being the mean distance over which a high-energy electron loses all but $1/e$ of its energy by bremsstrahlung

mass. Additionally, the cutoff wavelength of LiF is near 120 nm and so it does not limit the sensitive wavelength range. We have constructed and tested an HBD using this design principle as a prototype detector for the PHENIX experiment[20] (one of four experiments presently under construction at the Relativistic Heavy Ion Collider (RHIC) accelerator at Brookhaven National Laboratory). We describe here the design, construction, and successful testing of our prototype.

2 Detector Design

Here we present a brief description of the critical design details of the HBD. A more complete treatment can be found in the Master's Degree thesis of Mr. Robert Pisani[21].

2.1 Radiator Gas Vessel and Transparency Monitor

Shown in Figure 2 is the radiator vessel and gas flow diagram for the HBD. A mixed beam of electrons and negative pions enters the detector from the right. The entrance window is made from 50 μm thick Kapton which is aluminized on the interior side. Aluminization is necessary to prevent diffusion of water into the radiator gas and a subsequent loss in UV light transmission. After entering the detector the beam passes through the radiator gas volume traveling toward the photon detector. A movable "sail" is placed in the radiator tube and acts as a light block. Only light created downstream of the sail can reach the photon detector. The sail is mounted upon a magnetic base which allows it to be repositioned without breaking the radiator vessel seal.

The beam passes directly through the photon detector (described in detail below) and exits through a second aluminized Kapton window. The photon detector is mounted upon a large flange which acts as the back wall of the radiator vessel. The mounts for the radiator vessel windows accept exterior blankoffs for use when evacuating the vessel. The windows are pumped on both sides (exterior side through a valved line) to prevent implosion. High purity C_2F_6 gas (etching grade 99.95%) flows through a large Oxysorb cylinder prior to entry into the gas vessel. The gas enters near the beam entrance, flows along the radiator tube, and past the photon detector. After this, the gas flows through a second long tube labeled "transparency monitor"(TM) prior to bubbling through Si diffusion pump oil and out to air. The second tube is used to periodically check the transparency of the radiator gas. A Hamamatsu continuous D_2 lamp is mounted at one end of the TM. The wavelength of light sent into the gas volume is selected using one of three narrow bandpass filters

(124nm, 156nm 173nm).

After passing through the TM tube, the light level is measured by a photomultiplier tube with a MgF_2 entrance window. Transmission is measured by comparing the phototube current to that measured with the TM tube under vacuum. During data taking, the transmission was typically 90-95% at 156 nm.

2.2 Photon Detector

The design of the photon detector is driven by a variety of requirements. First and foremost is the requirement that the fragile LiF window not break. Care must be taken to mount the window in a stress free manner as well as to ensure that no significant difference in pressure develops between the avalanche and radiator gas volumes. The design must allow for a quick detector assembly after evaporation to minimize exposure of the cathode to air[14]. The cathode plane must be low mass and quite flat. Additionally, the cathode substrate must be chemically compatible with the CsI coating excluding a simple Cu-clad PC board[18].

Shown in Figure 3 is an exploded view of the detector. The beam enters from the top, passes sequentially through the LiF window, anode mesh, cathode, and finally exits through the vessel back window. The cathode is divided into 42 readout channels called pads. The LiF window is mounted in a “stress-eliminating fixture”. An aluminized Kapton ring is stretched between the outer mounting ring and the inner window support ring. The LiF is glued directly to the inner ring. In this “floating” configuration, stresses on the detector and the outer mounting ring result in twists or distortions of the Kapton and are not transferred to the window.

The anode grid consists of a stainless steel mesh with 50 μm wires and 500 micron spacing (81% transmission). The grid is stretched across a Cu-clad G10 ring and attached using a 95% tin-5%antimony solder with HCl acid flux. The cut edges of the G10 are painted with a low outgassing epoxy. High voltage (HV) contact is supplied by a set of four Au-plated spring contacts located around the perimeter of the pad plane. The cathode pad plane is printed on a 150 μm thick G10 circuit card. Plated-through holes of 250 μm diameter carry the signals to the back plane. Directly beneath the pad plane is a Minco Kapton foil heater used to bake the cathode after evaporation. The heater is followed by a carbon fiber-epoxy hexcell honeycomb and then a backing of another 125 μm sheet of G10. During construction, the pad plane is placed face down on a flat granite table. The hexcell sandwich serves to stiffen the pad plane without adding a significant amount of material to the detector .

The pad plane is cylindrically segmented as shown in Figure 4.

It has long been known that a CsI coating deposited upon Cu will readily form CuI and perform with a substantially reduced quantum efficiency[18]. Cu pads with an electroplated layer of Au have also been shown to be problematic due to the diffusion of Cu through the Au layer. Our pads used an electroless plating of Ni ($2.5\ \mu\text{m}$) followed by an electroless plating of Au ($0.125\ \mu\text{m}$) to become chemically compatible with the CsI layer. The Ni serves as a diffusion barrier to prevent migration of the Cu to the surface. The Au provides a chemically neutral substrate for the CsI layer. Recent work also indicates that a smooth micro-topography of the CsI layer is critical to the performance of the cathode and that the Ni/Au substrate induces an especially smooth surface growth pattern[18].

To make a properly functioning PPAC, it is imperative that the pad plane be not only flat but highly parallel to the HV grid. The grid cannot be permanently attached to the pad plane since it must be removed during the evaporation stage. However, if the anode mesh were attached instead to the upper lid, a large number of high precision pieces would have been necessary to ensure that the grid remained parallel to the pad plane. We have solved these problems using only a single precision piece, the grid spacer. A diagram of the anode mesh, grid spacer, and pad plane in its assembled form is shown in Figure 5. The upper and lower lid are machined in such a way that the nominal spacing in the absence of the grid spacer would be 0.6 mm. The grid spacer piece (1.6 mm thick) is placed between the grid and pad plane. During assembly, the grid is gently stretched across the grid spacer ring and automatically adjusts to be exactly parallel to the pad plane. Additionally, we have engineered the pad plane's hexcell stiffener so that under the unavoidable stresses created during assembly, the active area will not distort. As shown in Figure 5, the hexcell stiffener is sized to completely cover the active area and the region below the grid spacer, but does not extend to the outer edge of the pad plane circuit card. In this way, the outer regions of the circuit card absorb all necessary deflections (HV contact springs, forces from grid spacer, gas pressure differences across the pad plane) leaving the active area quite flat. Thus, in some sense, the active area of the pad plane is also in a floating fixture similar to that of the window. We feel that these considerations were crucial to achieving the high gain and excellent uniformity discussed below.

All items below the dashed line in Figure 3 are placed in the evaporator during deposition of the CsI layer. The lower lid is permanently attached to the back flange (which serves as the final seal of the radiator vessel). All signal connections are made (through to the feedthroughs) as well as high voltage, Kapton heater, and a thermo-couple. Quick assembly was aided by the configuration of the gas lines. Gas inlet and outlets flow through straight stainless steel tubes which are permanently attached to the upper lid as shown

in Figure 3. During assembly the tubes are inserted through bored out Cajon UltraTorr fittings (O-ring seal on tube exterior) permanently mounted in the vessel back flange. Assembly after deposition involved the following steps:

- (i) Place grid spacer on pad plane.
- (ii) Place anode mesh on spacer.
- (iii) Place upper lid on anode mesh (LiF window already attached) and bolt in place.
- (iv) Insert completed detector into radiator vessel.

The entire procedure took less than 10 minutes. Both the photon detector and the radiator vessel were tested with a He leak detector and registered no leak to its most sensitive setting (10^{-9} cm³/sec).

2.3 CsI Deposition

The CsI deposition was performed at Stony Brook. Our techniques are based upon the prescriptions set by the Fermi National Accelerator Laboratory's (FNAL) Particle Detector Group (PDG)[17]. The bell jar used a large diffusion pump, which was protected against backflush of oil by a liquid nitrogen cold trap. Extensive cleaning of the bell jar was performed prior to our use. Evaporations were typically performed at a vacuum level of $7-8 \times 10^{-8}$ torr. The cathode was warmed gently during deposition via the embedded heater foil (one watt produced equilibrium temperatures between 45 and 50° C).

The CsI was evaporated directly from scintillator grade crystals resting in a molybdenum boat. A movable shutter was placed above the boat. The shutter was closed as the boat was first warmed so that the initial deposition was only to the back of the shutter. CsI was deposited simultaneously onto the cathode and a quartz crystal thickness monitor. The 5000Å continuous layer was deposited in roughly 90 seconds. After deposition, the evaporator was let up to UHP grade nitrogen (not air). The cathode maintained at 45° C during this procedure and its removal from the bell jar. We believe that the temperature significantly retards condensation during the time that the cathode is handled in air.

To date we have made roughly a dozen cathodes. Each of these was measured to have a quantum efficiency equal to those made for us in the past by the PDG at FNAL, 20-25% at 190 nm.

2.4 Gas Flow Topology

Shown in Figure 6 is the gas flow system. Most characteristics are quite standard and will not be discussed in detail. All bubblers in the system use a Si diffusion pump oil with a vapor pressure of $< 10^{-10}$ torr. The key design goal of the system is to separate the avalanche and radiator volumes while avoiding a differential pressure buildup across the window. This is accomplished quite simply by bubbling the avalanche gas directly into the radiator volume. The pressure drop across the 1mm depth of the avalanche gas bubbler is less than one torr. The flow requirements in either volume are specified in turnovers per unit time. Since the detector interior volume is roughly 1% of the radiator's volume, less than a 1% contamination of the radiator gas at equal turnover rates is experienced. This level of contamination is not enough to significantly alter the index of refraction of the radiator gas or change the transparency characteristics of the whole system (radiator and avalanche gas combined).

3 Bench Tests

Bench tests were conducted upon the final detector and on a single cell prototype. The tests were performed to verify the quality of the cathodes, test various avalanche mixtures, and estimate the quantum efficiency of the cathode used for the beam test.

3.1 Quantum Efficiency Measurement

The apparatus used for quantum efficiency measurement is the same as that used in a previous publication[7]. The style of the measurement is similar to many used by others[14]. A flash lamp is attenuated to the point of fewer than 0.1 photo-electrons per flash. Data are taken at a single wavelength for the PMT and for the chamber. The ratio of the count rates in the two devices establishes the ratio of their quantum efficiencies. As noted previously, our apparatus provides a relative measurement of quantum efficiency since the PMT used is not calibrated on an absolute scale. The tube used has a reflective cathode (these cathodes have less variability in QE than the transmission type). We assign a 25% systematic error to the QE measurement as recommended by the manufacturer of the tube[22].

Over the past few years, several cathodes were made for us Anderson and collaborators. Each of these cathodes was measured by us to have a quantum efficiency in the range 20-25% at 190 nm (consistent with the publications of

that group). Each of the cathodes made at Stony Brook was measured to have a quantum efficiency of 21-23% at 187 nm. The cathode used for the beam test has shown no measurable deterioration in QE over the two month period since initial deposition.

3.2 *Avalanche Gas Mixture Tests*

Our plan had been to use a $He+CF_4$ mixture for the avalanche gas, as originally prescribed by Giomataris and Charpak[23]. However, our tests showed that even at low concentration, the CF_4 still acted to steal the signal. The size of a single avalanche using a 5% CF_4 mixture was among the largest signals of the signals we measured; however, the quantum efficiency was lowered by roughly a factor of four. One cathode was tested with ethane, then $He+5\% CF_4$ and then again with ethane. The QE dropped from 22% to 2%, and returned to 15% after reintroduction of ethane. Although different electric field strengths could minimize the electron capture probability, further tests with CF_4 were not pursued.

Helium is an optimal choice for the principle component of the radiator gas due to its small dE/dx (0.31 keV/cm) which minimizes the signal from non-radiating charged particles. A number of possible quenchers were tried in the hope of finding a mixture with transparency down to 120 nm. Such a choice was not found in our tests. Our final choice for the avalanche gas was $He + 5\% CH_4$ since methane is the most transparent of the hydrocarbons (down to 140 nm at our low concentration and short length)[24]. Helium is quite easy to quench since the principle photon feedback lines are quite deep in the VUV, near 65 nm wavelength. Methane in concentrations as low as 1% yields a high gain avalanche.

It has been known for some time that the use of a noble gas in the avalanche mixture can have detrimental effects on the net quantum efficiency of the cathode (a factor of 4–10 reduction)[25]. This effect has been primarily associated with the reflection of the photoelectron back into the cathode via elastic collisions with the noble gas atoms. These effects have been specifically observed in association with CsI cathodes[13,14], leading us to expect similarly poor results with our He based mixture. In all those tests, [13,14,25], the current produced from the cathode was measured under exposure to a (relatively) bright light source with the cathode under low electric field. We have performed tests of the cathode quantum efficiency in the presence of a noble gas mixture using the single photo-electron approach described above.

We first measured the quantum efficiency of a cathode using pure ethane as the avalanche gas. This particular gas choice gives especially high gain since it

is more strongly quenched than pure methane. The vessel was then evacuated and filled with the 95% He+5% methane mixture. We measured the quantum efficiency to be reduced by only 10% while using the noble gas mixture. We suggest that the strong electric field (> 5000 V/cm) may have restored the quantum efficiency in the presence of the noble gas.

3.3 Gain Uniformity

The uniformity of the gain across the 12cm detector surface was inspected using the UV light source. Bright light flashes (thousands photons per flash) were scanned across the entire surface of the detector. Response (the product of gain and quantum efficiency) was monitored by measuring the pulse height from the anode. A maximum variation of less than 10% was observed.

4 Beam Tests

The HBD detector was tested at the Brookhaven National Laboratory's Alternating Gradient Synchrotron (AGS). The 29 GeV/c primary proton beam was incident upon a thick production target. The B2 test beam line views that target with a double focusing momentum analyzing spectrometer. A Pb sheet was placed at the entrance of B2 to induce photon conversions and increase the fraction of electrons present in the beam.

Just prior to the second analyzing magnet, the beam passed through a scintillator paddle (S2) and a Cherenkov detector (C1). After the magnet, the beam passed through a second Cherenkov detector (C2) and another scintillator paddle (S3). The beam passed directly through the HBD and was finally incident upon a 6 x 6 x 18 inch Pb-glass block (PBGL). A small scintillator (1x1 cm, S4) was placed before the PBGL counter and ensured that the incident beam particle landed near the center of the PBGL. The trigger selected charged particles passing through S2, S3, and S4. Electron identification was performed by analysis of the beam Cherenkov and PBGL detectors offline.

Clean electrons were defined by demanding a proper pulse height in each scintillator, firing of both Cherenkov counters, and full energy deposit in the PBGL counter. Clean pions were defined by demanding proper pulse height in each scintillator, pedestals in both Cherenkov detectors and "punch-through" in the PBGL counter. The HBD was **not used** in the event selection. A cathode pad was defined as having been struck if that pad's pulse height was greater than 3.5 sigma above the pedestal.

Three data sets were taken with the C_2F_6 radiator. The first used a radiator length of 1.2 meters, the second 80 cm, and the third 40 cm. Lengths were set by repositioning the light blocking sail. Unfortunately, just prior to the 1.2 meter length running a low purity (99.0%) bottle of CF_4 was run through the radiator vessel. The transparency monitor registered only 2/3 transmission at 156 nm while running this bottle. Although the transmission recovered to roughly 90% during the C_2F_6 run, it is suspected that some residual contamination may have reduced transmission and consequently detector performance at other wavelengths. Such possible contaminations were not present during the shorter radiator length tests.

Figure 7 shows the response of the detector to electrons. In this figure, we have plotted the first 25 electron events in sequence from a C_2F_6 run at 120 cm length. Shaded pads are those defined as struck under the criteria listed above. Electrons clearly fire numerous pads on a single event. Figure 8 shows the detector's response to the first 25 pion events in sequence from the same tape. Zero or one struck pad is the most likely response of the detector to the passage of a pion.

The results in Figure 9 are accumulated over all available data at the 120 cm radiator length. The top panel shows the probability of a given number of pads firing. Pions are represented by the solid line and electrons by the dashed line. The mean number of pads fired per pion is 0.6 with a most likely number of zero. Electrons fire a mean of ten pads. The bottom panel shows the spectrum of pulse heights measured by the digitization of the anode pulse height. Again, excellent separation of electrons and pions is apparent. These two variables (anode pulse height and number of pads) can be plotted in the form of a scatter plot as shown in top panel of Figure 10. Here blue crosses represent the detector response to particles that the beam logic identified as electrons, and red open circles represent the response to pions. The separation between pions and electrons is apparent. Also shown in this figure are the results at the 80cm and 40cm runs. The statistics for the 80 and 40cm runs were much lower than that of the 120 cm run because of operating complications with the AGS during our test run.

Two aspects of the detector response distinguish electrons from pions: total charge deposited and number of pads fired. It is instructive to analyze the rejection power of each of these measures independently. First, we consider the limit of an unsegmented or coarsely segmented detector in which the only possible separation technique is pulse height. Electrons would be chosen by requiring a total charge deposit above a certain threshold. Both the electron efficiency and the pion contamination will be a function of the threshold. The crosses in Figure 11 show the pion efficiency vs. the electron efficiency achieved by various cuts on anode pulse height. We can generate a series of such curves by additionally adding cuts on the minimum number of pads fired.

These curves are also shown in Figure 11. The best chamber performance is achieved by a combination of both cuts. At 95% electron efficiency, the pion efficiency is 1/333. At 90% electron efficiency, the pion efficiency is 1/910. Similar analyses can be performed on the data sets for the 80 cm and the 40 cm radiator lengths (see figure 10). Figures 12 show the analysis performed on the 80 cm radiator length data. Figures 13 show the result for the 40 cm radiator length runs. Table 1 summarizes the results of pion rejection at the three lengths of radiator for both 95% and 90% electron efficiency at 1 GeV/c momentum.

5 Considerations Regarding Cherenkov Light Produced in the Window

At normal incidence, Cherenkov light produced in the window is totally internally reflected and thus does not contribute to the pion signal. Such is not the case at non-normal incidence. Part of the Cherenkov cone will be transmitted through the window. We have done a detailed calculation to estimate the strength of the window Cherenkov signal from the window as a function of angle. The following factors were considered:

- (i) The fraction of the Cherenkov photons which are not internally reflected varies as a function of the charged particle's incident angle.
- (ii) The fraction of Cherenkov photons which penetrate the anode grid varies as a function of photon angle.
- (iii) The distance over which the charged particle radiates (length of the medium) varies with incident angle (distance = thickness/cos(θ)).
- (iv) The index of refraction in the window[26] and quantum efficiency of the cathode both vary as a function of wavelength.

The solid line in top panel of Figure 14 shows the fraction of Cherenkov photons which are not internally reflected as a function of incident angle of the charged particle. The peak "transmittance" is 40%. The dashed line in the same figure is the fraction of Cherenkov photons which both leave the window and are transmitted through the anode grid. These calculations can be folded with the Cherenkov spectrum and quantum efficiency of the cathode to determine the mean number of photo-electrons produced at the cathode as a function of the charged particle's incident angle. This result is shown as the solid line in the bottom panel of Figure 14. For most incident angles the Cherenkov light produces fewer than a single photo-electron. Further reduction in the signal can be accomplished by additional collimation placed behind the window. We have modeled the effect of a 1mm thick piece of hexcell with a 5 mm cell size placed behind the window. In this case, the signal yield is 0.6 photo-electrons, less than the mean produced from other sources.

We conclude that the Cherenkov signal from the window is small and can be made smaller by simple manipulations. Future prototypes will be constructed so that a variety of incident angles can be experimentally tested.

6 Summary

We have designed, constructed, and successfully tested a hadron blind detector. The detector varies from the original design of Giomataris and Charpak by the introduction of a crystal window to separate the radiator and avalanche volumes. By choosing LiF (the lowest Z crystal in nature) we have added minimal thickness to the detector and maintained maximal transparency. The window allows for flexibility in the radiator gas choice, eliminating concerns about avalanche characteristics and chemical mischief in the presence of the cathode. We have developed a stress eliminating fixture and gas flow topology (bubbling detector gas into the radiator) to protect the window against breakage.

We have developed a thin yet high and uniform gain PPAC using the hexcell sandwich technique. The cathode plane has an embedded heater and thermocouple useful for warming the cathode during CsI deposition and vacuum baking. The PPAC assembles quickly (drop in parts, HV spring contacts, slide-in gas fittings) and includes a self-aligning feature ensured by the grid spacer ring. The pad plane uses Ni and Au electroless plating to make it chemically compatible with the CsI overcoating.

We have successfully produced high quality cathodes at Stony Brook using no extraordinary measures beyond cleanliness, good vacuum, and warming of the cathode during and after deposition.

We have tested the HBD in a beam of electrons and negative pions using a C_2F_6 radiator (high n, good transparency) and a helium (low dE/dx) methane avalanche gas mixture. Pion rejection was measured as a function of radiator length with results summarized in Table 1. Effective pion rejection at high electron efficiency has now been demonstrated in a compact, thin package (radiator lengths as short as 40 cm).

Acknowledgement

We would like to extend our heartfelt and extreme thanks to David Anderson, Simon Kwan, and all our friends in the FNAL Particle Detector Group. Without their steadfast and accurate advise and help we would not have reached

this stage in our research. We also thank Dr. Craig Woody for generous loans of equipment and advice. We thank Brant Johnson for juggling the testbeam schedule after our low purity bottle of CF_4 was discovered. All data at 80 cm and 40 cm lengths were taken during time he found “in the margin”. We thank Dave Dayton, Alan Carroll, and everyone in the AGS crew for their assistance during our run. We like to thank Dr. Min Chen for the loan of equipment and a postdoc during our testrun. We also wish thank Mr. Richard Hutter for technical advice during the project and Sergey Panitkin for all help while setting up our computers systems. This work was supported in part by the United States Department of Energy grant #431-8321A.

References

- [1] Y. Giomataris and G. Charpak, Nucl. Instr. and Meth. A310 (1991) 589.
- [2] D.F. Anderson, S. Kwan, and V. Peskov, Nucl. Instr. and Meth. A 343 (1994) 109.
- [3] E. Aprile, A. Bolotnikov, D. Chen, et al., Nucl. Instr. and Meth. A 343(1994) 129.
- [4] C. Lu and K.T. McDonald Nucl. Instr. and Meth. A343 (1994) 135.
- [5] C. Coluzza, J. Almeida, H. Berger, et al., Nucl. Instr. and Meth. A 343 (1994) 152.
- [6] H. Brauning, A. Breskin, et al., Nucl. Instr. and Meth. A348 (1994) 223.
- [7] B. Surrow, T. Hemmick, et al., Nucl. Instr. and Meth. A355 (1994) 342.
- [8] A. Braem, A DiMauro, et al., Nucl. Instr. and Meth. A 343 (1994) 163.
- [9] R. Aleksan, P. Besson, Ph. Bourgeois, et al., Nucl. Instr. and Meth. A343 (1994) 173.
- [10] M. Staric, V. Cindro, S. Korpar, et al., Nucl. Instr. and Meth. A343 (1994) 192.
- [11] J. Seguinot, G. Charpak, Y. Giomataris, et al., Nucl. Instr. and Meth. A297 (1990) 133.
- [12] B. Hoeneisen, D Anderson, S Kwan, Nucl. Instr. and Meth. A302 (1991) 447
- [13] V. Dangendorf, A. Breskin, R. Chechik, et el., Nucl. Instr. and Meth. A308 (1991) 519.
- [14] D.F. Anderson, S. Kwan, V. Peskov, and B. Hoeneisen, Nucl. Instr. and Meth. A323 (1992) 626.
- [15] R. Enomoto, T Sumiyoshi, and Y. Fujita, Nucl. Instr. and Meth. A 343 (1994) 117.

- [16] G. Malamud, Ph Mine, D. Vartsky, et al., Nucl. Instr. and Meth. A348 (1994) 275.
- [17] D.F. Anderson, S Kwan, and V. Peskov, Nucl. Instr. and Meth. A326 (1993) 611.
- [18] J. Almeida, F. Barbo, M Bertolo, et al., Nucl. Instr. and Meth. A361 (1995) 245.
- [19] A. Breskin, R. Chechik, et al., Nucl. Instr. and Meth. A 343 (1994) 159.
- [20] PHENIX Conceptual Design Report, Brookhaven National Laboratory, 29 January 1993.
- [21] Robert Pisani, *Design, Construction, and Successful Testing of a Hadron Blind Detector*, (1995).
- [22] Hamamatsu engineer, private communication.
- [23] Y. Giomataris, G Charpak, V. Peskov, and F. Sauli, Nucl. Instr. and Meth. A323 (1992) 431.
- [24] H. Okabe and D.A. Becker, J. Chem. Phys. 39 (1963) 2549.
- [25] D.F. Anderson, R. Bouclier, G. Charpak, et al., Nucl. Instr. and Meth. 217 (1983) 217.
- [26] W. Driscoll, *Handbook of Optics*, McGraw-Hill Book Co., New York (1978).

Table 1: Pion rejection as a function of radiator length

RadiatorLength(cm)	$\epsilon_{\text{electron}} = \mathbf{0.95}$	$\epsilon_{\text{electron}} = \mathbf{0.90}$
40	1/100	1/140
80	1/150	1/333
120	1/333	1/910

Figure 1: The top panel shows the Cherenkov Detector suggested by Charpak and Giomataris. The lower panel shows our altered design.

Figure 2: Radiator Vessel and gas flow for the HBD.

Figure 3: Exploded View of the Photon Detector.

Figure 4: Cylindrical segmentation of the cathode pad plane.

Figure 5: Diagram of PPAC region after assembly.

Figure 6: Gas flow topology of the entire system.

Figure 7: HBD response to the first 25 electrons on tape from a random run. Mean number of pads which fires is 10.

Figure 8: HBD response to the first 25 Pions on tape from a random run. Mean number of pads which fire is .6.

Figure 9: Top panel shows the probability of a given number of pads firing. The bottom panel shows the spectrum of the pulse height measured by digitization of the anode.

Figure 10: Shows the Electron and Pion separation of the 120, 80, and 40 cm radiator lengths by plotting the number of pads which fire vs the total collected charge on the anode. The blue crosses are the detectors response to ELECTRONS in the trigger logic and the red circles are the detectors response to PIONS in the trigger logic.

Figure 11: Detectors efficiency curves generated by cutting on the number of pads fired and anode pulse height for the 1.2 meter length.

Figure 12: Detectors efficiency curves generated by cutting on the number of pads fired and anode pulse height for the 0.8 meter length.

Figure 13: Detectors efficiency curves generated by cutting on the number of pads fired and anode pulse height for the 0.4 meter length.

Figure 14: The solid line in top panel of this figure shows the fraction of Cherenkov photons which are not internally reflected as a function of incident angle of the charged particle. The dashed line in the same figure is the fraction of Cherenkov photons which both leave the window and are transmitted through the anode grid. The bottom panel shows the mean number of photo-electrons produced as a function of the particles incident angle.

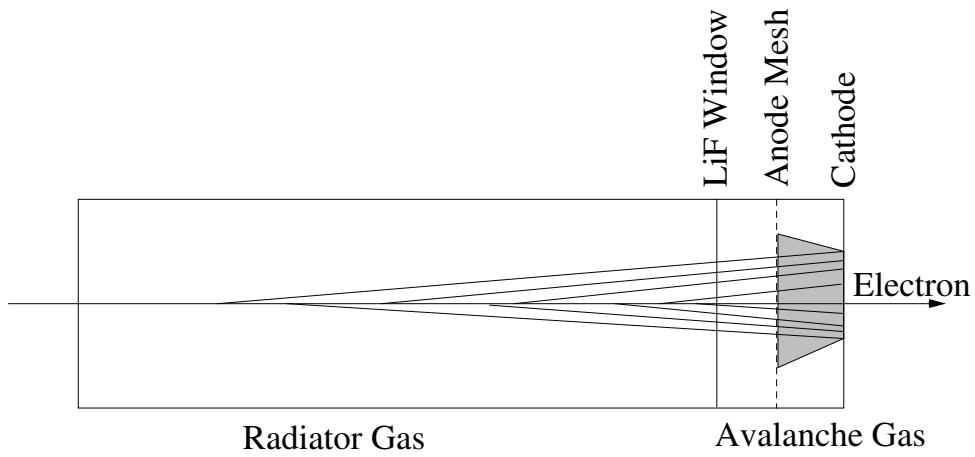
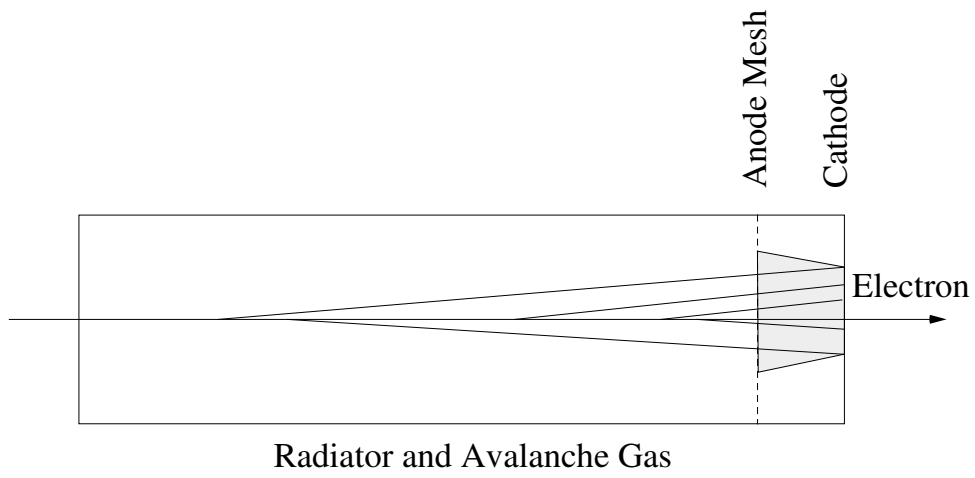


Fig. 1.

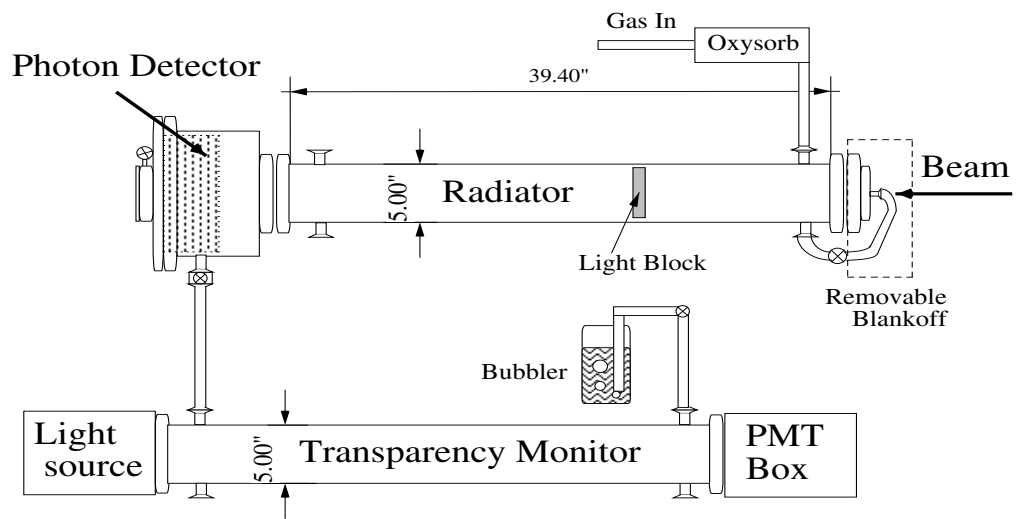


Fig. 2.

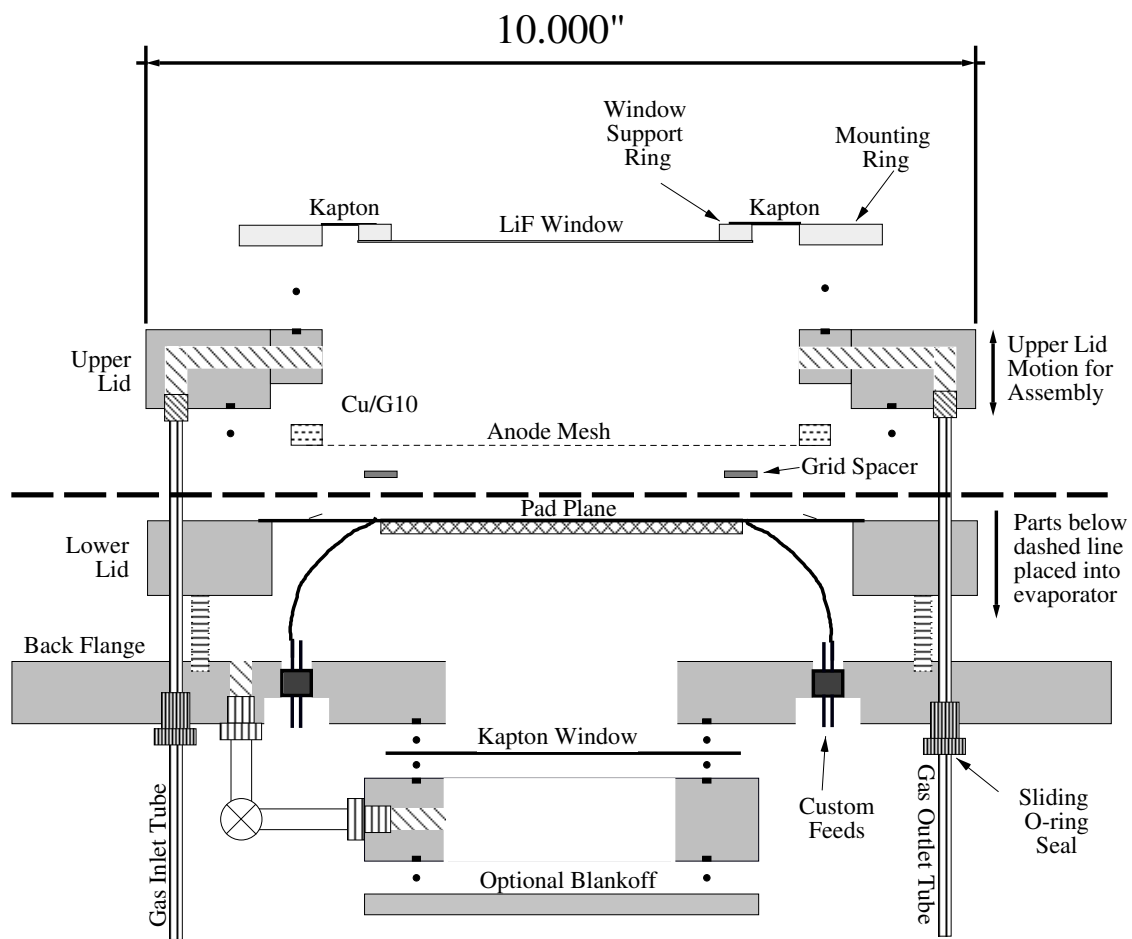


Fig. 3.

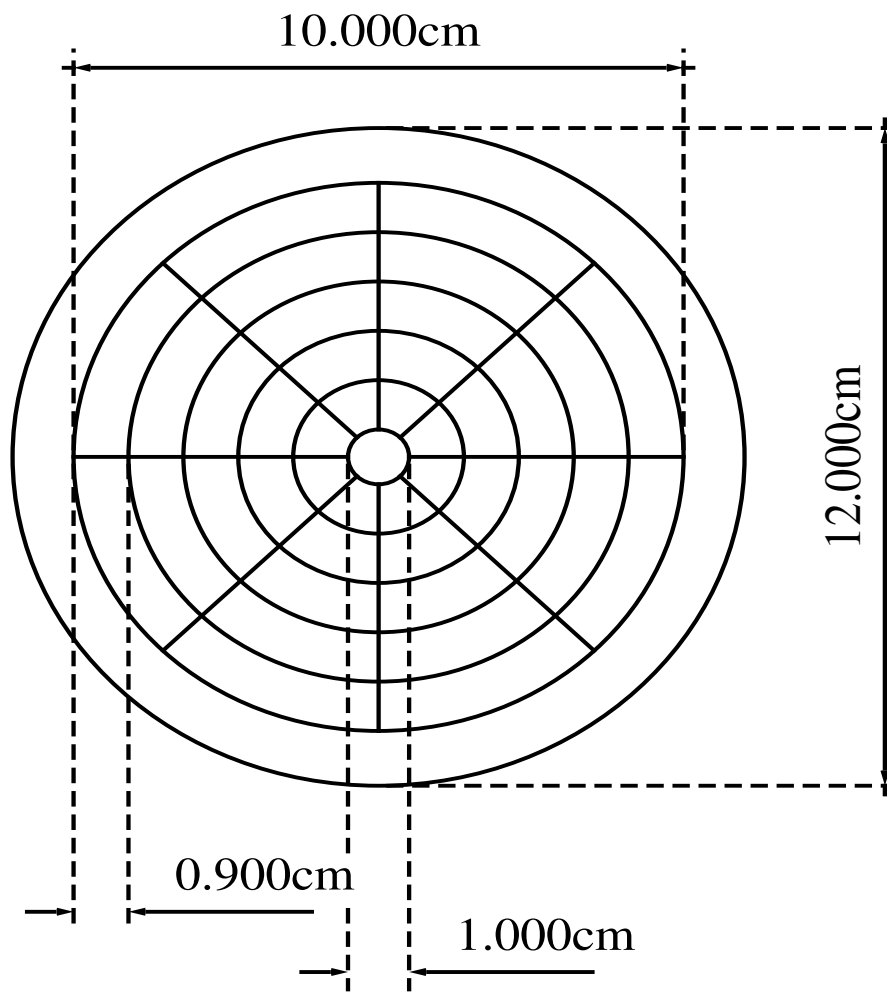


Fig. 4.

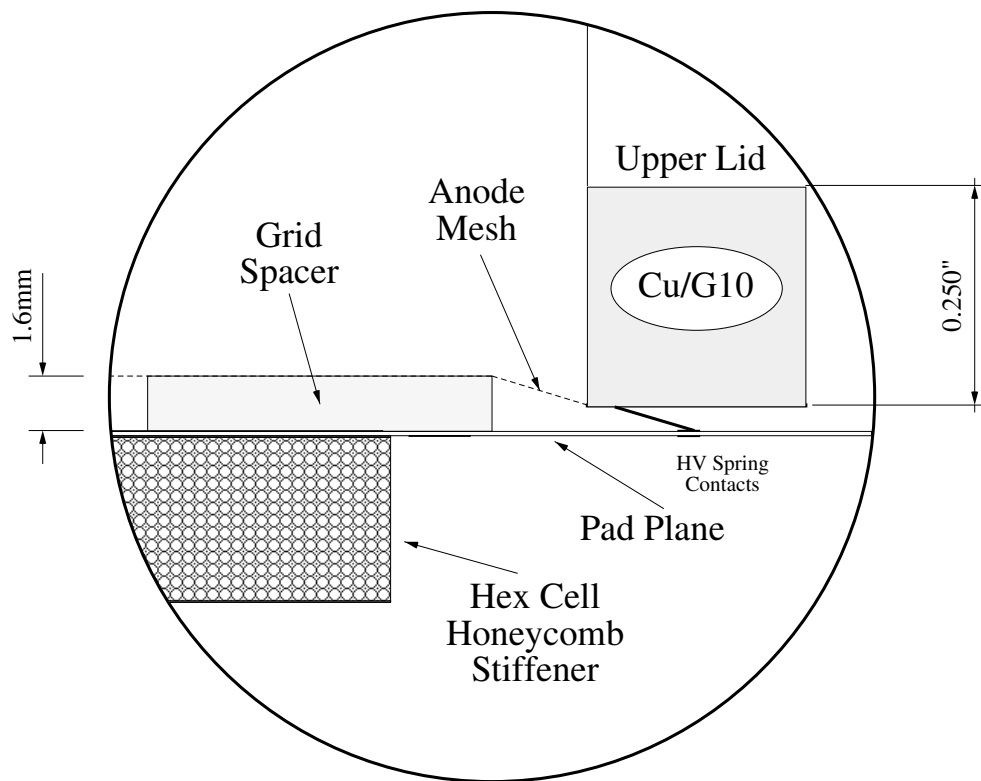


Fig. 5.

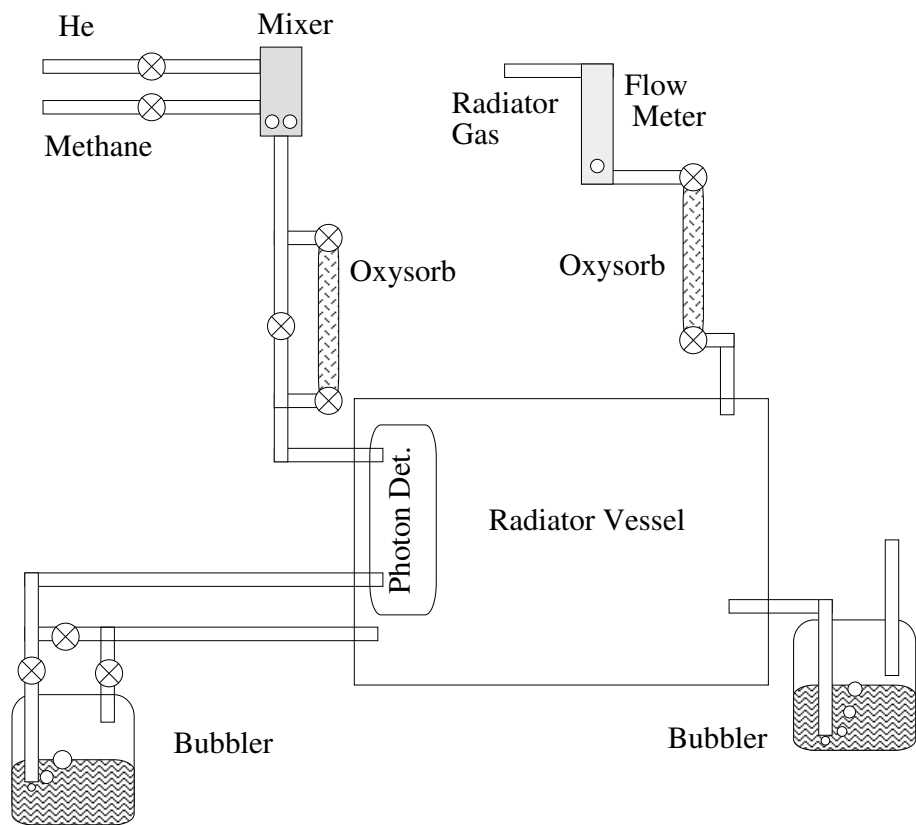
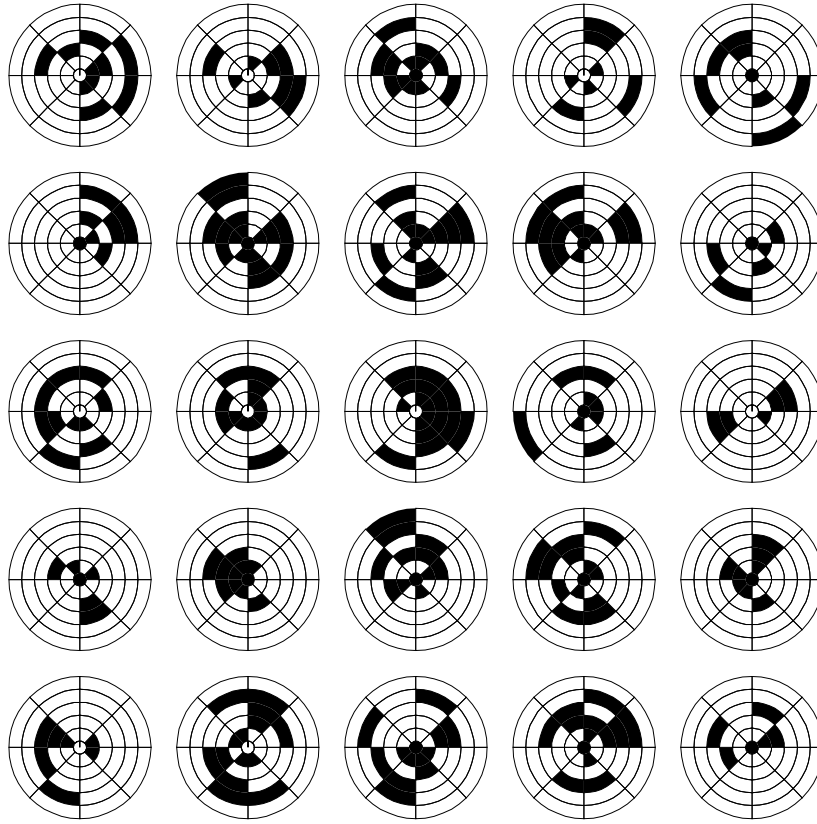


Fig. 6.

PHENIX HBD Display



Next	Open Meta	Hard Copy	Close Meta	N-Displays	Elec Color	Pion Color	HBD Color	End
------	-----------	-----------	------------	------------	------------	------------	-----------	-----

Fig. 7.

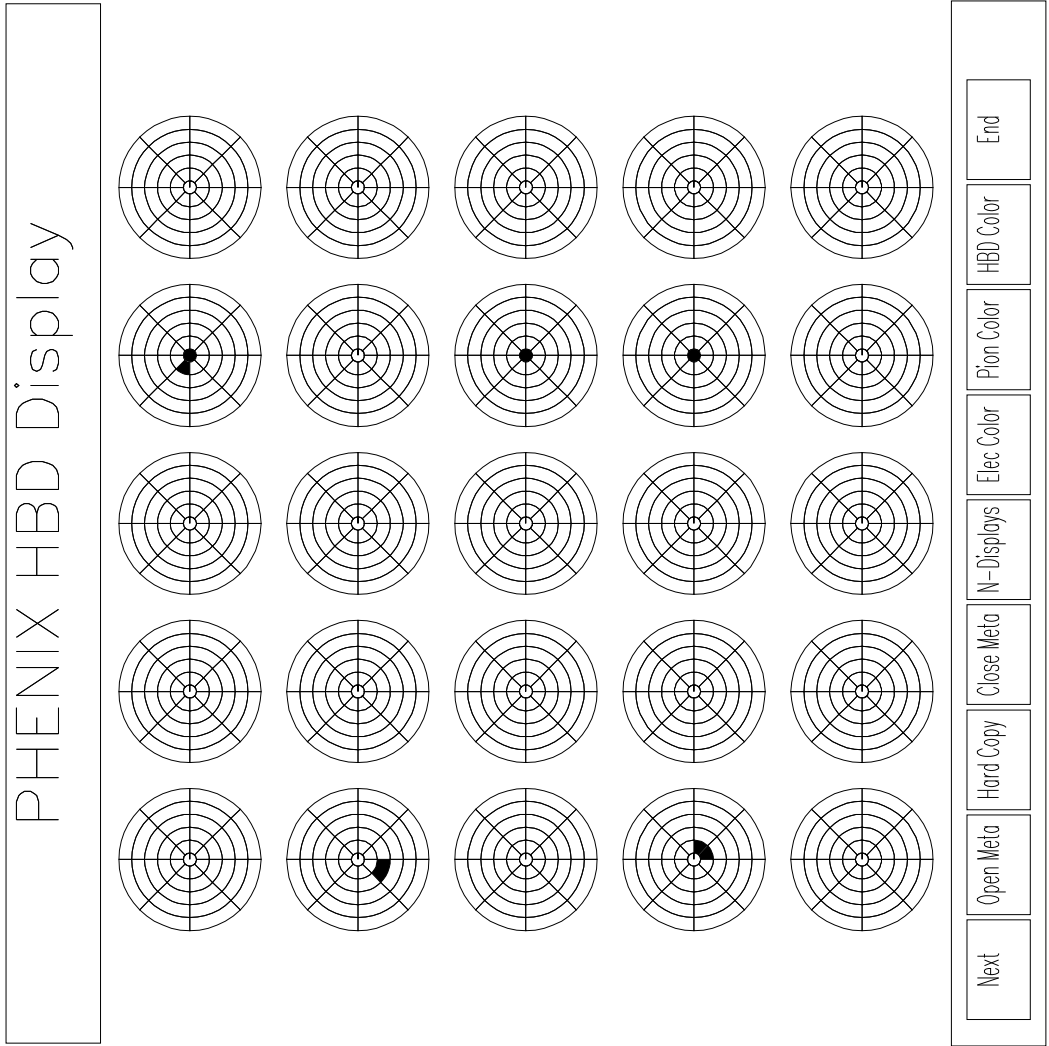


Fig. 8.

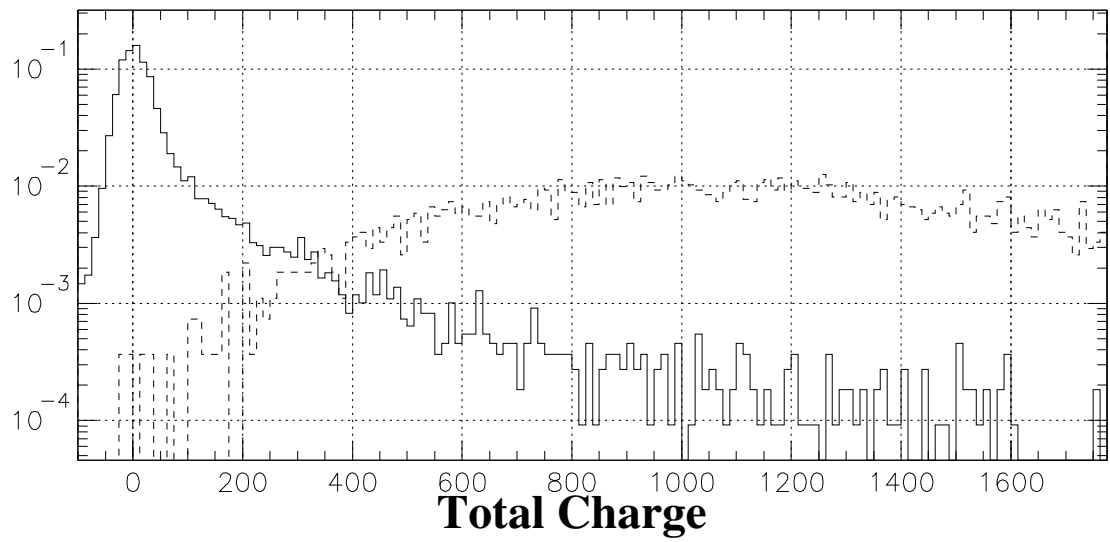
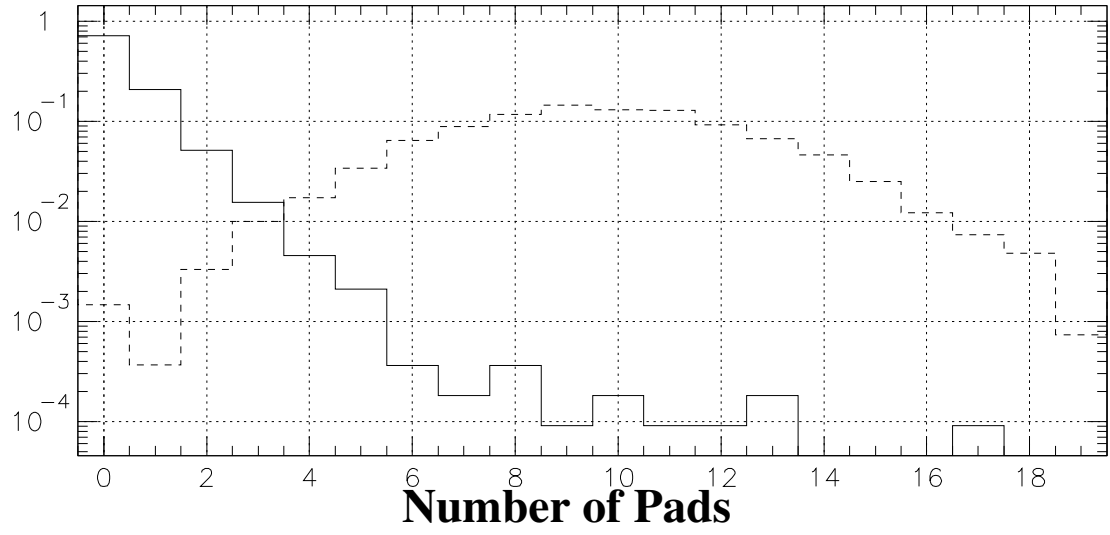


Fig. 9.

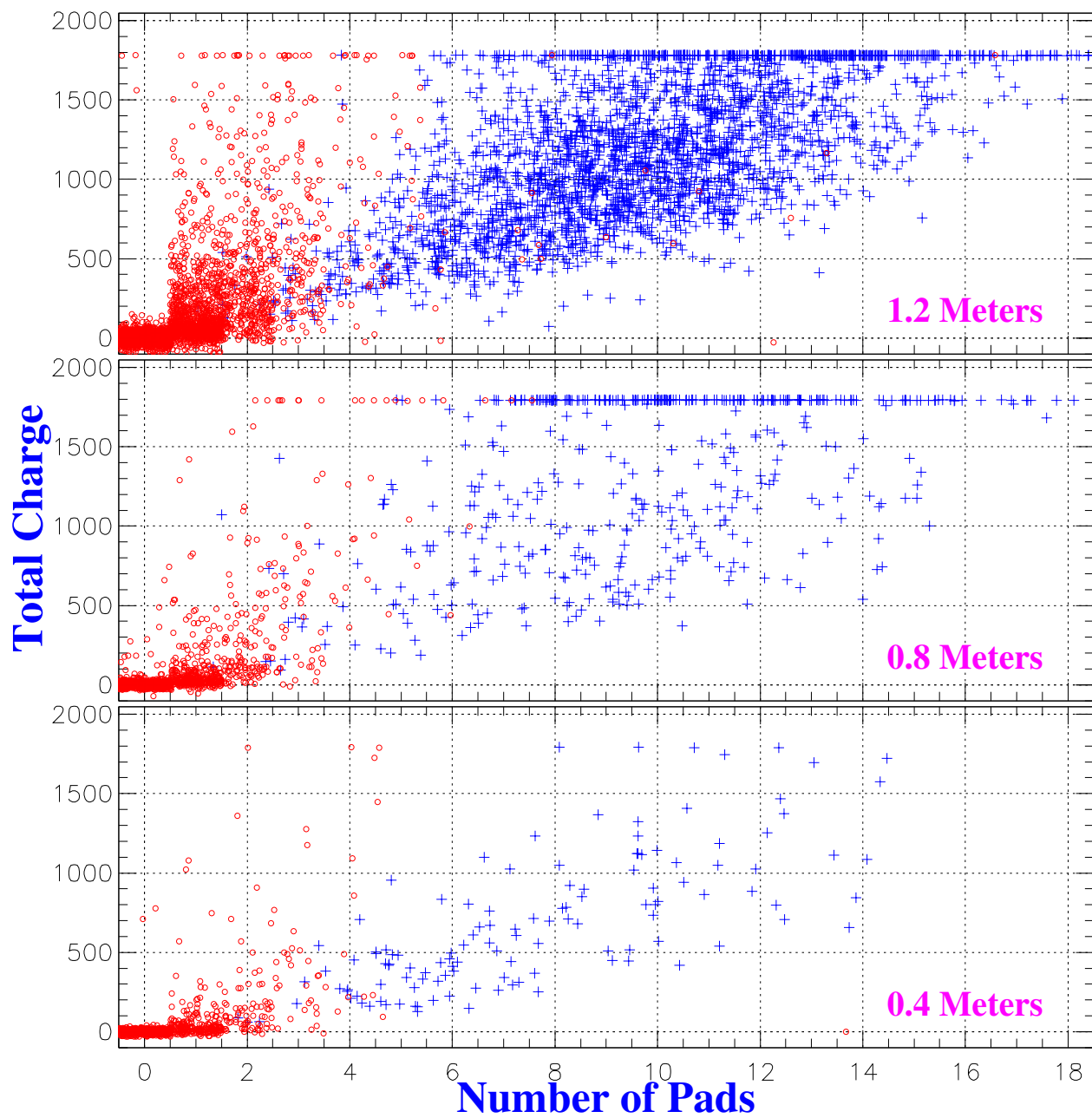


Fig. 10.

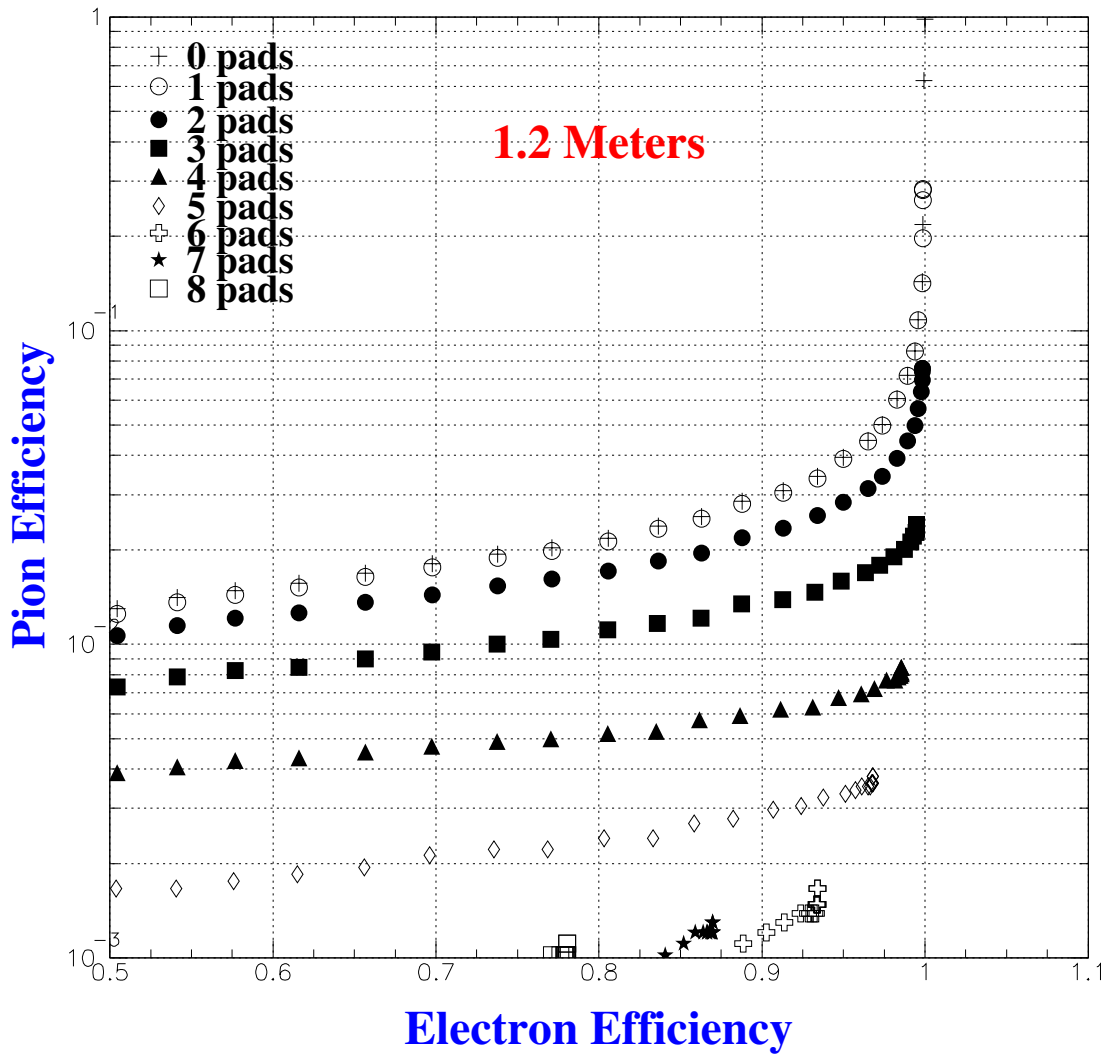


Fig. 11.

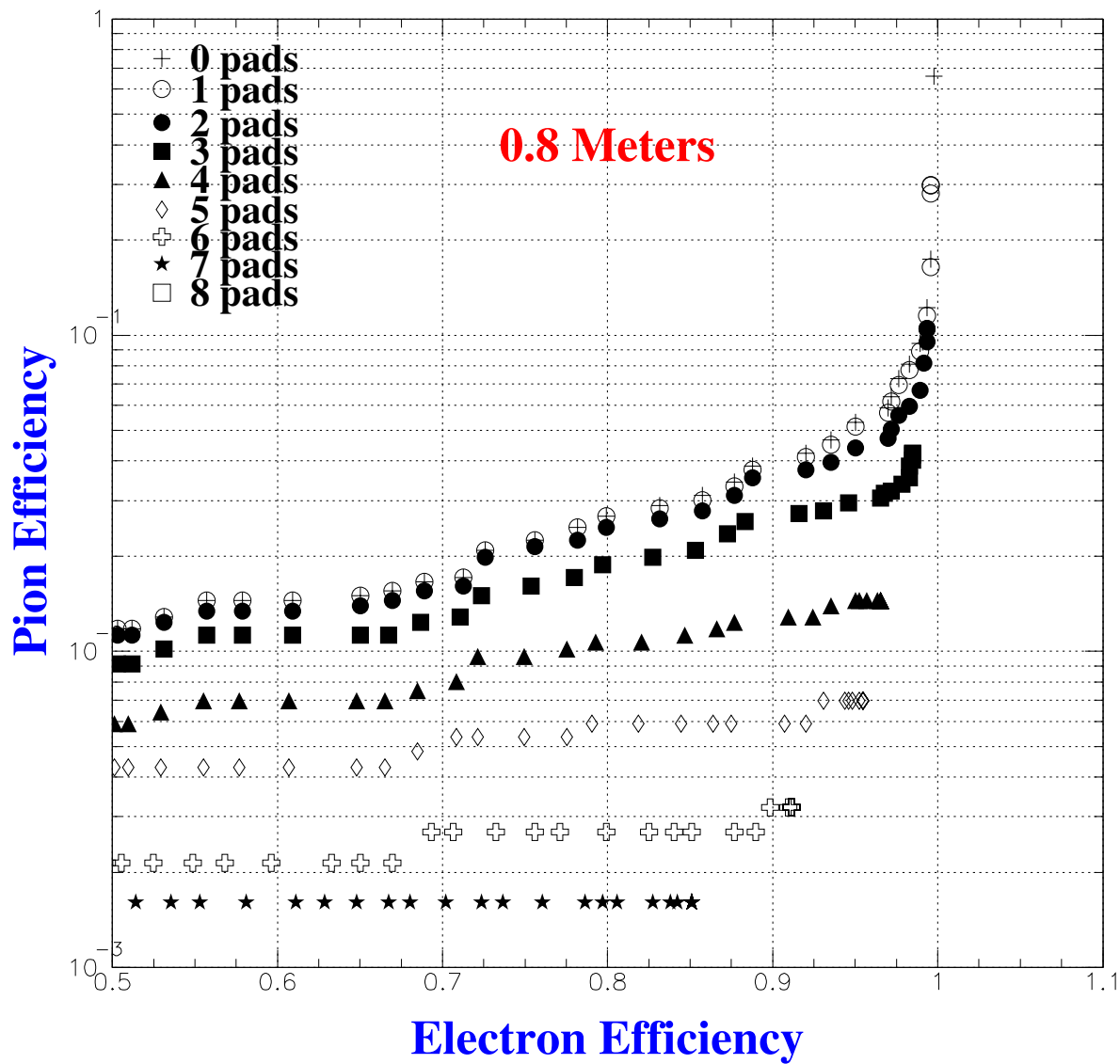


Fig. 12.

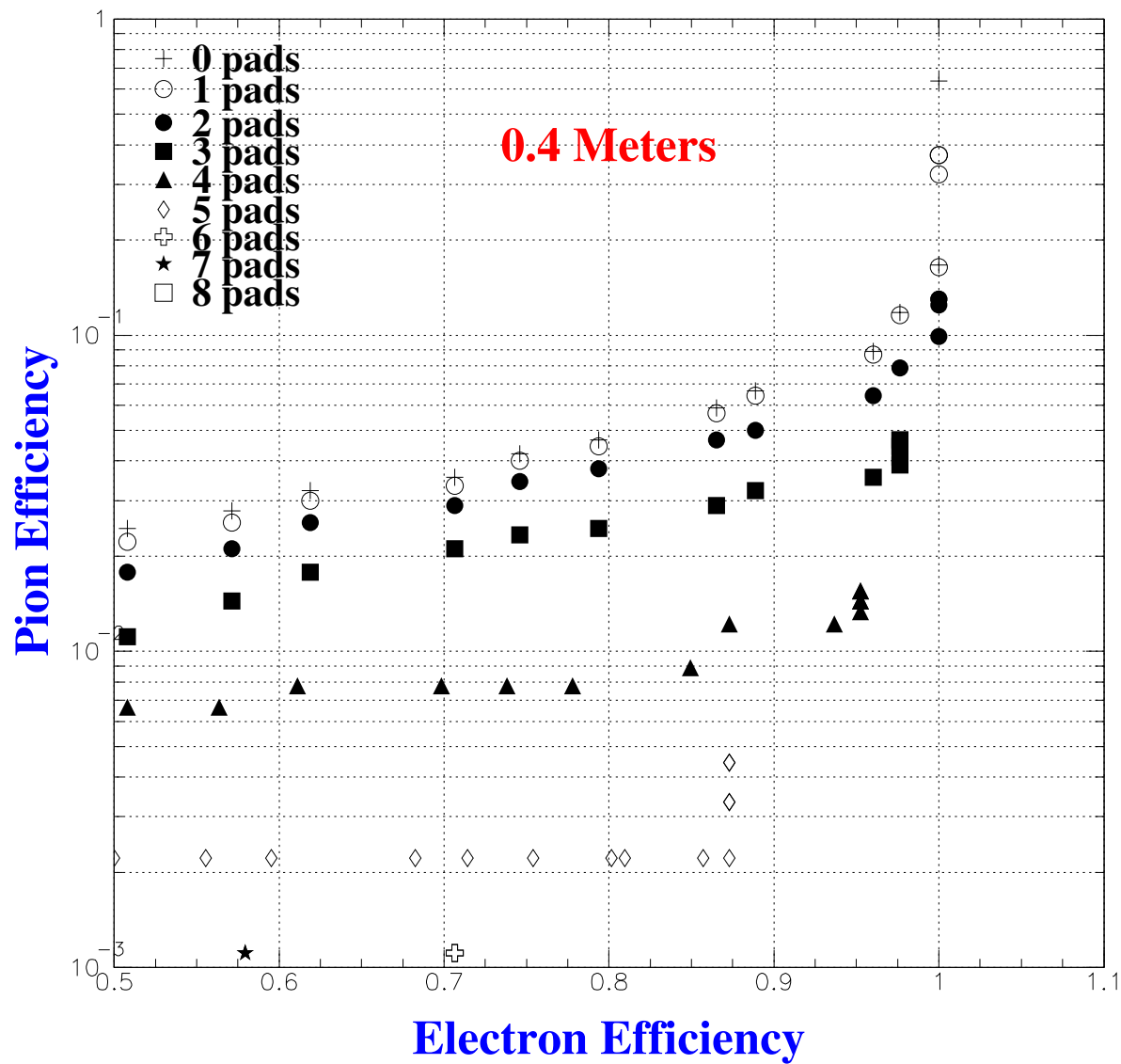


Fig. 13.

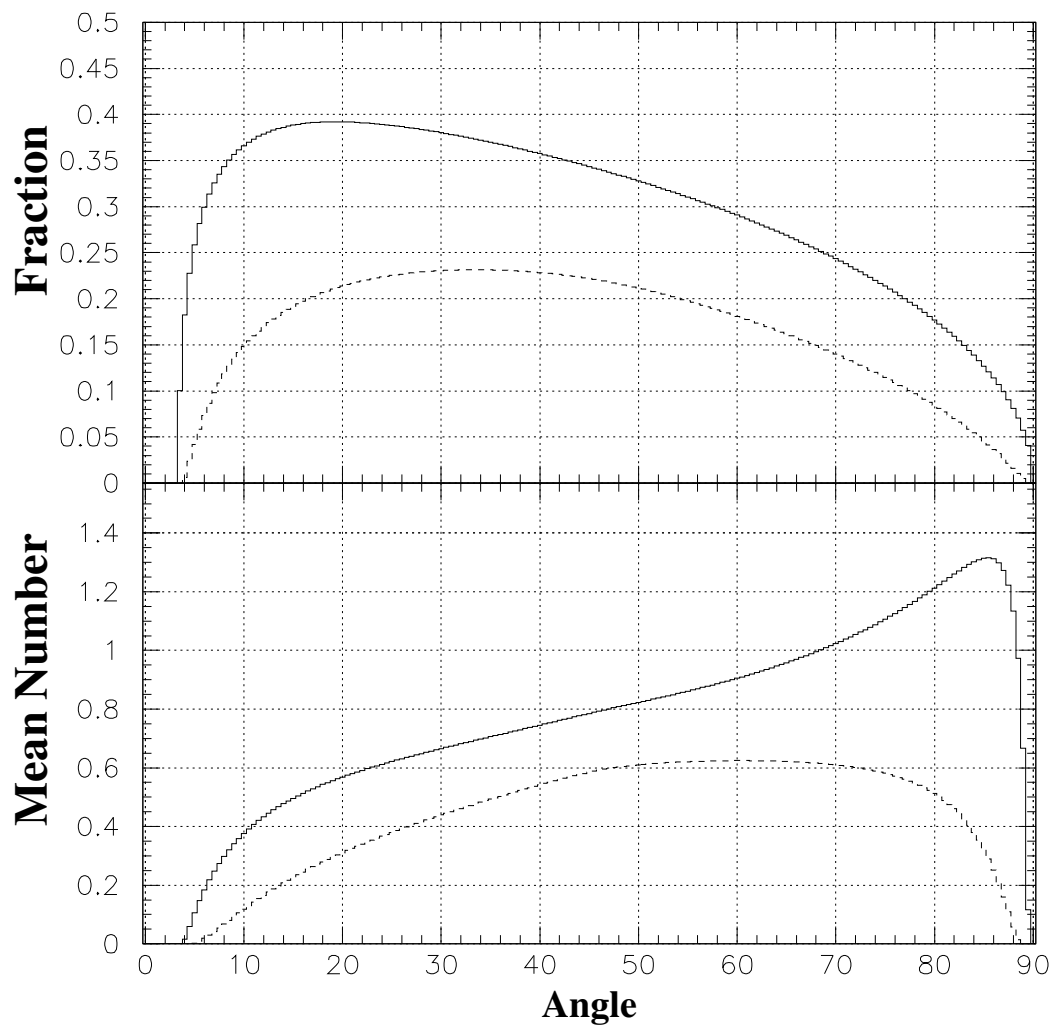


Fig. 14.